chemistry

MDPI

Article

Anti-Orthopoxvirus Activity of Amantadine and Rimantadine Derivatives—In Vitro Testing and Molecular Modeling

Ivan A. Moskalev [1], Ekaterina A. Akishina [2], Evgenij A. Dikusar [2], Olga I. Yarovaya [3,*], Sophia S. Borisevich [1], Edward M. Khamitov [4], Alexey Yu. Fedorov [1], Sergey G. Arkhipov [1,*], Nikolay I. Bormotov [5], Olga A. Serova [5], Larisa N. Shishkina [5], Vladimir. I. Potkin [2] and Nariman F. Salakhutdinov [3]

[1] SRF "SKIF", 630559 Koltsovo, Russia; i.a.moskalev@srf-skif.ru (I.A.M.); s.s.borisevich@srf-skif.ru (S.S.B.); a.yu.fedorov@srf-skif.ru (A.Y.F.)
[2] Institute of Physical Organic Chemistry, National Academy of Sciences of Belarus, 220072 Minsk, Belarus; che.semenovaea@mail.ru (E.A.A.); evgen_58@mail.ru (E.A.D.); potkin@ifoch.bas-net.by (V.I.P.)
[3] Department of Medicinal Chemistry, N.N. Vorozhtsov Novosibirsk Institute of Organic Chemistry SB RAS, Lavrentyev av. 9, 630090 Novosibirsk, Russia; anvar@nioch.nsc.ru
[4] Laboratory of Physicochemical Methods of Analysis, Ufa Institute of Chemistry, Ufa Federal Research Centre of the Russian Academy of Sciences, 69 Prospekt Oktyabrya, 450054 Ufa, Russia; khamitovem@gmail.com
[5] State Research Center of Virology and Biotechnology VECTOR, Rospotrebnadzor, 630559 Koltsovo, Russia; bormotov_ni@vector.nsc.ru (N.I.B.); serova.olga.a@yandex.ru (O.A.S.); shish@vector.nsc.ru (L.N.S.)
* Correspondence: ooo@nioch.nsc.ru (O.I.Y.); arksergey@gmail.com (S.G.A.)

Abstract: In 2022, the number of mpox cases spiked worldwide, leading to a surge in scientific research on members of the *Orthopoxvirus* genus and the discovery of new compounds exhibiting anti-orthopoxvirus activity. This work is devoted to the synthesis of compounds containing an adamantane fragment and the evaluation of their activity against the vaccinia virus, offering a possible mechanism of the antiviral action of the synthesized agents. Among all the studied adamantane derivatives, three compounds (**2**, **4**, and **12**) were found to demonstrate the highest antiviral activity, with the most promising compound **2** (N-(adamantan-1-yl)isonicotinamide) having the lowest toxicity level with a selectivity index (SI) of 115. The pharmacophoric profiles of these compounds are similar to the pharmacophoric profile of tecovirimat, an inhibitor of the membrane viral protein p37. Analysis of the results of molecular modeling suggests that the investigated compounds can inhibit the vaccinia virus by suppressing the phospholipase activity of membrane viral protein p37.

Keywords: adamantane; amides; antiviral activity; orthopoxvirus; membrane viral protein p37; molecular docking; molecular dynamic

check for updates

Academic Editors: Athina Geronikaki, Cosimo D. Altomare and Maria Stefania Sinicropi

Received: 14 January 2025
Revised: 25 February 2025
Accepted: 26 February 2025
Published: 1 March 2025

Citation: Moskalev, I.A.; Akishina, E.A.; Dikusar, E.A.; Yarovaya, O.I.; Borisevich, S.S.; Khamitov, E.M.; Fedorov, A.Y.; Arkhipov, S.G.; Bormotov, N.I.; Serova, O.A.; et al. Anti-Orthopoxvirus Activity of Amantadine and Rimantadine Derivatives—In Vitro Testing and Molecular Modeling. *Chemistry* **2025**, *7*, 34. https://doi.org/10.3390/chemistry7020034

Copyright: © 2025 by the authors. Licensee MDPI, Basel, Switzerland. This article is an open access article distributed under the terms and conditions of the Creative Commons Attribution (CC BY) license (https://creativecommons.org/licenses/by/4.0/).

1. Introduction

After continuous global vaccination efforts, the eradication of smallpox was officially declared in 1980, and this event was considered one of the greatest public health achievements in history [1]. This eradication was possible largely due to the fact that the variola virus causing smallpox is entirely human-specific. In May 2022, there was a surge in mpox cases in different countries across the globe [2]. Mpox (formerly known as monkeypox) virus (MPXV) belongs to the genus *Orthopoxvirus* (OPXV) and the family *Poxviridae*, which includes such other dangerous viruses as variola virus (VARV, causing smallpox), cowpox virus (CPXV), and vaccinia virus (VACV) [3]. Until 2022, MPXV was recognized as a zoonosis endemic to African countries, and cases of human-to-human transmission were rarely reported [4,5]. Since May 2022, MPXV outbreaks caused by human-to-human transmission

have rapidly spread, with more than 94,200 confirmed cases in more than 100 countries [6]. As a result, the World Health Organization (WHO) has declared a public health emergency of international concern.

Because of the growing concern about the spread of zoonotic orthopoxviruses or the use of smallpox or monkeypox virus in biological warfare or bioterrorism [7], the search for chemotherapeutic agents with activity against orthopoxviruses is becoming an extremely urgent task for medicinal chemistry and virology [8]. ST-246 (Tecovirimat, TPOXX®) (Figure 1), developed by SIGA Technologies Inc. (New York, NY, USA), is approved in the United States for the treatment of smallpox and mpox [9,10]. In Russia, the compound NIOCH-14, a prodrug of tecovirimat, is registered as an official drug against smallpox with a similar mechanism of action to that of tecovirimat [11]. Another small-molecule drug for the treatment of smallpox in humans, CMX001 (Brincidofovir), was approved by the U.S. Food and Drug Administration (FDA) in June 2021 [12,13]. Brincidofovir is a lipophilic analog of cidofovir (Cidofovir, CDV, Vistide®) (Figure 1), an antiviral drug used to treat cytomegalovirus retinitis, which also demonstrates activity against orthopoxvirus infection in both mice and monkeys [14,15]. Cidofovir was previously shown to have low oral bioavailability and significant nephrotoxicity. It was also found to be ineffective when used after the onset of smallpox lesions in VARV-infected monkeys. In its turn, brincidofovir was shown not to provide a sufficient level of protection against ectromelia virus (ECTV, causing mousepox) infection in the experiments with small rodents [16].

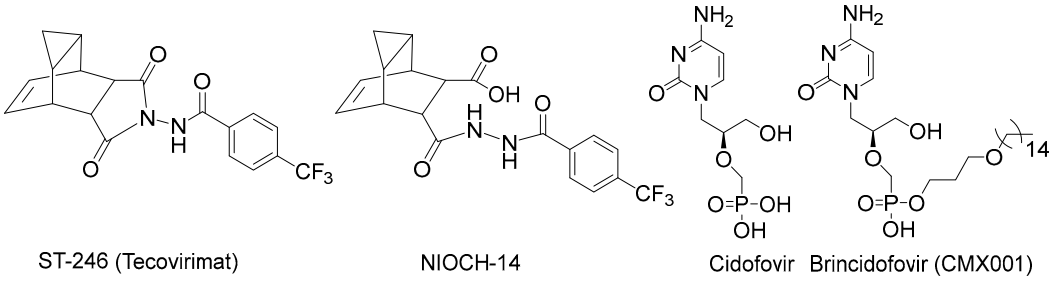

Figure 1. Compounds currently approved for the treatment of VARV.

Aminoadamantanes, such as amantadine, rimantadine, tromanatadine, and memantine, have a broad spectrum of biological activity and have firmly established themselves in the pharmaceutical market [17]. They have shown high therapeutic potential against viral diseases, as well as in the treatment of diseases of the central nervous system [18,19]. The best-known influenza virus ion channel inhibitors were widely used in flu therapy prior to the emergence of resistant strains [20]. When adamantane fragments are incorporated into the structure of existing compounds, they improve the pharmacokinetic properties of the modified compounds, often increasing their biological activity [21,22]. In particular, the in vitro and in vivo activity of rimantadine was recently demonstrated against SARS-CoV-2 omicron variant virus [23] and an ion channel inhibitor of Zika virus [24]. A series of adamantane derivatives were also reported to exhibit activity against vaccinia virus [25]. It was also found that amine conjugates based on monoterpenes and 1-adamantane carboxylic acids have high activity against a wide range of orthopoxviruses [26]. A synthesis and investigation of the activity against orthopoxviruses for a wide range of aromatic amides containing adamantane fragments are described in [27]. A separate study of a series of aromatic amides based on 1- and 2-adamantanamine as inhibitors of orthopoxviruses showed the importance of a substituent in the para-position of the aromatic fragment [28]. In addition, the significance of the amide or N-acyl-hydrazone bond between the natural fragment's backbone and the aromatic ring was demonstrated [29].

The antiviral activity of adamantane derivatives may be related to the inhibition of the viral membrane protein p37 [27]. The p37 protein is a highly conserved peripheral membrane protein encoded by the F13L gene [30], which consists of 372 amino acids and has a molecular weight of 41.8 kDa. The expression of the p37 protein occurs in the late stages of infection [31]. The protein targets the membranes originating from the Golgi apparatus, where it is incorporated into the virion during the wrapping of intracellular mature viral particles. It should be noted that the viral protein p37 is inhibited by a drug that is effective against a number of orthopoxviruses, tecovirimat [32]. Previously, the authors of the paper [27] used the adamantane fragment based on van der Waals volume considerations of the "cage", comparing it to the "cage" fragment of tecovirimat, an inhibitor of the membrane viral protein p37 [32]. The molecule design contained a donor–acceptor fragment and an aromatic ring with a substituent in the para-position. According to the results of structural studies of tecovirimat and some of its analogs, the electron-donor properties of substituents in the aromatic ring influence the EC_{50} value [33]. The results of the publication [33], as well as the studies of the mechanism of antiviral activity of adamantane derivatives described in Reference [28], suggest that new compounds containing an adamantane fragment could inhibit the phospholipase activity of protein p37.

In this work, we studied both previously described adamantane derivatives and new compounds containing an adamantane moiety. As initial structures, we used 1-adamantane amine and rimantadine. The synthesized compounds include aromatic and heteroaromatic fragments.

2. Materials and Methods

2.1. Chemistry

General Information

All chemicals were purchased from commercial suppliers and used without any further purification, unless otherwise indicated. IR spectra were recorded on a Thermo Nicolet Protege 460 Fourier Transform spectrometer (Nicolet, MA, USA) using KBr pellets as the sample. ^{1}H and ^{13}C NMR spectra were acquired on a Bruker Avance 500 spectrometer (Bruker, MA, USA, 500 and 125 MHz, respectively) in $CDCl_3$ and DMSO-d6. The residual solvent signals ($CDCl_3$, δ_H 7.26, δ_C 77.2 ppm; DMSO-d6, δ_H 2.50, δ_C 40.1 ppm) were used as internal standards. The assignment of signals in the ^{13}C NMR spectra was performed using the DEPT technique. Liquid chromatography–mass spectrometry spectra were recorded on an Agilent 1200 LC-MS system with an Agilent 6410 Triple Quad Mass Selective Detector (Agilent, MA, USA) with electrospray ionization in the positive ion registration mode (MS2 scanning mode). An Agilent ZORBAX Eclipse XDB-C18 (Agilent, MA, USA, 4.6 × 50 mm, 1.8 μm) column was used, and the mobile phase MeCN–H_2O + 0.05% HCO_2H with gradient elution from 40 to 90% MeCN in 10 min was used. A flow rate of 0.5 mL/min was used. Elemental analysis was performed on a Vario MICRO cube CHNS analyzer (Elementar, MA, USA). Melting points were determined on a Kofler bench.

General Procedure for the Synthesis of Amides **1**–**3**. Triethylamine (4.1 mmol) and hydrochloride of 2-phenyl-4-quinolinecarboxylic/nicotinic/isonicotinic acid chloride (2 mmol) were added to a solution of 2 mmol of 1-adamantylamine in methylene chloride. The mixture was stirred for 8 h and left at room temperature for 12 h, then washed with water and a 5% aqueous $NaHCO_3$ solution. The organic layer was separated, dried over Na_2SO_4, and filtered, and the solvent was evaporated. The product was purified by recrystallization from a mixture of ether and hexane.

N-(Adamantan-1-yl)nicotinamide (**1**): yield 80%; mp 167–168 °C; IR (KBr) ν 3358 (NH), 3075 (C-H_{Ar}), 2917, 2905, 2890, 2850 (C-H_{Aliph}), 1658 (C=O), 1594, 1528, 1477, 1455, 1419,

1361, 1343, 1309, 1259, 1201, 1166, 1094, 1032, 741, 699 cm^{-1}; ^1H NMR ($CDCl_3$, 500 MHz) δ 1.64–1.75 (6H, m, $3CH_{2adam}$), 2.07–2.15 (9H, m, $3CH_{adam}$ + $3CH_{2adam}$), 5.93 (1H, br.s, NH), 7.31 ($1H_{Py}$, ddd, J = 12.7, 4.8, 0.8 Hz), 8.00–8.04 ($1H_{Py}$, m), 8.64 ($1H_{Py}$, dd, J = 4.8, 1.5 Hz), 8.70 ($1H_{Ar}$, d, J = 1.8 Hz); ^{13}C NMR ($CDCl_3$, 125 MHz) δ 29.56 ($3CH_{adam}$), 36.41 ($3CH_{2adam}$), 41.71 ($3CH_{2adam}$), 123.50 ($1CH_{Py}$), 135.02 ($1CH_{Py}$), 147.86 ($1CH_{Py}$), 151.91 ($2CH_{Py}$), 52.86, 131.70, 164.83 (C=O) ($3C_{quater}$); Anal. calcd. for $C_{16}H_{20}N_2O$ (256.34):C, 74.97; H, 7.86; N. 10.93%; Found: C, 75.11; H, 8.15; N, 10.79%.

N-(Adamantan-1-yl)isonicotinamide (**2**): yield 63%; mp 128–130 °C; IR (KBr) ν 3418 (NH), 3043 (C-H_{Ar}), 2905, 2849 (C-H_{Aliph}), 1645 (C=O), 1577, 1553, 1491, 1453, 1408, 1360, 1345, 1307, 1285, 1261, 1104, 1088, 1000, 843, 756, 685 cm^{-1}; ^1H NMR ($CDCl_3$, 500 MHz) δ 1.64–1.75 (6H, m, $3CH_{2adam}$), 2.05–2.15 (9H, m, $3CH_{adam}$ + $3CH_{2adam}$), 6.00 (1H, br.s NH), 7.51 ($2H_{Py}$, dd, J = 6.0, 1.5 Hz), 8.63 ($2H_{Py}$, dd, J = 6.0, 1.4 Hz); ^{13}C NMR ($CDCl_3$, 125 MHz) δ 29.51 ($3CH_{adam}$), 36.35 ($3CH_{2adam}$), 41.56 ($3CH_{2adam}$), 120.95 ($2CH_{Py}$), 150.45 ($2CH_{Py}$), 52.94, 143.16, 164.72 (C=O) ($3C_{quater}$). Anal. calcd. for $C_{16}H_{20}N_2O$ (256.34): C, 74.97; H, 7.86; N. 10.93%; Found: C, 81.09; H, 8.05; N, 10.87%.

N-(Adamantan-1-yl)-2-phenylquinoline-4-carboxamide (**3**): yield 78%, mp 258–260 °C; IR (KBr) ν 3316 (NH), 3068 (C-H_{Ar}), 2902, 2848 (C-H_{Aliph}), 1644 (C=O), 1593, 1539, 1455, 1354, 1344, 1296, 118, 1158, 1094, 1029, 884, 768, 689 cm^{-1}; ^1H NMR ($CDCl_3$, 500 MHz) δ 1.70–1.80 (6H, m, $3CH_{2adam}$), 2.14–2.19 (3H, m, $3CH_{adam}$), 2.19–2.24 (6H, m, $3CH_{2adam}$), 5.91 (1H, br.s, NH), 7.44–7.55 ($4H_{Ar}$, m), 7.72 ($1H_{Ar}$, ddd, J = 15.3, 6.9, 1.4 Hz), 7.76 ($1H_{Ar,}$ s), 8.06–8.11 ($3H_{Ar}$, m), 8.14 ($1H_{Ar}$, d, J = 8.3 Hz); ^{13}C NMR ($CDCl_3$, 125 MHz) δ 29.65 ($3CH_{adam}$), 36.45 ($3CH_{2adam}$), 41.81 ($3CH_{2adam}$), 116.26 ($1CH_{Ar}$), 125.10 ($1CH_{Ar}$), 127.26 ($1CH_{Ar}$), 127.65 ($2CH_{Ar}$), 129.02 ($2CH_{Ar}$), 130.12 ($1CH_{Ar}$), 130.18 ($1CH_{Ar}$), 53.55, 123.47, 139.08, 144.15, 148.76, 156.98, 166.99 (C=O) ($7C_{quater}$); Anal. calcd. for $C_{26}H_{26}N_2O$ (382.50): C, 81.64; H, 6.85; N, 7.32%; Found: C, 81.77; H, 6.93; N, 7.15%.

N-(Adamantan-1-yl)-4,5-dichloroisothiazole-3-carboxamide (**4**). To a solution of 2 mmol of 1-adamantylamine in 5 mL of dry pyridine at room temperature, 2 mmol of 4,5-dichloroisothiazolecarboxylic acid chloride was added, and the reaction mixture was refluxed for 6 h, before being poured into 150 mL of an aqueous solution of sodium chloride and acidified with hydrochloric acid to pH 5. The precipitate was filtered off, washed with warm water, and dried in a vacuum over P_2O_5. Yield 78%, mp 132–133 °C; IR (KBr) ν 3343, 3288 (NH), 3072 (C-HAr), 2907, 2848 (C-H), 1677, 1660 (C=O), 1546, 1450, 1357, 1348, 1292, 1277, 1241, 1078, 968, 863, 749, 719, 646, 628, 601, 528, 509 cm^{-1}; ^1H NMR ($CDCl_3$, 500 MHz) δ 1.64–1.75 (6H, m, $3CH_{2adam}$), 2.07–2.14 (9H, m, $3CH_{adam}$ + $3CH_{2adam}$), 6.84 (1H, br.s, NH); ^{13}C NMR ($CDCl_3$, 125 MHz) δ 29.55 ($3CH_{adam}$), 36.42 ($3CH_{2adam}$), 41.53 ($3CH_{2adam}$), 52.63, 124.90, 150.42, 157.53, 158.03 (C=O) ($5C_{quater}$); Anal. calcd. for $C_{14}H_{16}Cl_2N_2OS$ (331.26): C, 50.76; H, 4.87; Cl, 21.40; N, 8.46; S, 9.68%; Found: C, 50.85; H, 5.02; N, 2.89; Cl, 21.29; N, 8.31; S, 9.55%.

General Procedure for the Synthesis of Imines **5**–**9**. A solution of 3.00 mmol of aldehyde, 3.05 mmol of rimantadine hydrochloride, and 1.60 mmol of K_2CO_3 in 30 mL of anhydrous methanol was refluxed for 24 h. The mixture was cooled, and the precipitate was filtered, washed with a small amount of cold methanol, and dried in vacuum.

N-(1-(Adamantan-1-yl)ethyl)-1-(5-phenylisoxazol-3-yl)methanimine (**5**)*:* yield 70%, mp 87–88 °C; IR (KBr) ν 3150, 3063, 2968, 2904, 2847, 1651 (C=N), 1613, 1590, 1572, 1497, 1451, 1373, 1361, 1344, 1314, 1112, 1093, 1041, 1022, 948, 934, 916, 809, 794, 765, 689 cm^{-1}; ^1H NMR (DMSO-d6, 500 MHz) δ 1.05 (3H, d, J = 6.5 Hz, CH_3), 1.41–1.49 (3H, m, $3CH_2$), 1.52–1.60 (6H, m, $3CH_2$), 1.61–1.68 (3H, m, $3CH_2$), 1.89–1.95 (3H, m, 3CH), 2.93 (1H, q, J = 6.5 Hz, CH_3CHN), 7.29 ($1H_{isox}$, s), 7.47–7.58 ($3H_{Ar}$, m), 7.93–7.97 ($2H_{Ar}$, m), 8.37 (1H, s, CH=N); ^{13}C NMR (DMSO-d6, 125 MHz) δ 16.15 (CH_3), 28.55 (3CH), 37.37 ($3CH_2$), 38.97 ($3CH_2$), 75.80 (CH_3CHN), 98.41 (CH_{isox}), 126.38 ($2CH_{Ar}$), 129.84 ($2CH_{Ar}$), 131.25 ($1CH_{Ar}$), 150.40

(CH=N), 35.94, 127.12, 163.12, 170.30 ($4C_{quater}$); MS *m*/*z* (I_{rel}, %) 335.10 $[M+H]^+$ (100); Anal. calcd. for $C_{22}H_{26}N_2O$ (334.46): C, 79.00; H, 7.84; N, 8.38%; Found: C, 79.13; H, 7.91; N, 8.31%.

N-(1-(Adamantan-1-yl)ethyl)-1-(5-(p-tolyl)isoxazol-3-yl)methanimine (**6**): yield 75%, mp 107–108 °C; IR (KBr) ν 3150, 3029, 2922, 2904, 2846, 1652 (C=N), 1618, 1594, 1567, 1509, 1449, 1372, 1359, 1344, 1313, 1249, 1114, 1092, 1037, 1020, 948, 940, 880, 822, 804 cm^{-1}; ^1H NMR (DMSO-d6, 500 MHz) *δ* 1.04 (3H, d, *J* = 6.4 Hz, CH_3), 1.39–1.47 (3H, m, $3CH_2$), 1.48–1.58 (6H, m, $3CH_2$), 1.59–1.67 (3H, m, $3CH_2$), 1.87–1.92 (3H, m, 3CH), 2.34 (3H, s, CH_3), 2.89 (1H, q, *J* = 6.5 Hz, CH_3CHN), 7.18 ($1H_{isox}$, s), 7.30 ($2H_{Ar}$, d, *J* = 7.9 Hz), 7.80 ($2H_{Ar}$, d, *J* = 7.9 Hz), 8.33 (1H, s, CH=N); ^{13}C NMR (DMSO-d6, 125 MHz) *δ* 16.13 (CH_3), 21.60 (CH_3), 28.56 (3CH), 37.37 ($3CH_2$), 38.96 ($3CH_2$), 75.79 (CH_3CHN), 97.71 (CH_{isox}), 126.31 ($2CH_{Ar}$), 130.36 ($2CH_{Ar}$), 150.39 (CH=N), 35.92, 124.47, 141.15, 163.05, 170.45 ($5C_{quater}$); MS *m*/*z* (I_{rel}, %) 349.20 $[M+H]^+$ (100); Anal. calcd. for $C_{23}H_{28}N_2O$ (348.49): C, 79.27; H, 8.10; N, 8.04%; Found: C, 79.31; H, 8.15; N, 7.95%.

N-(1-(Adamantan-1-yl)ethyl)-1-(4-((5-(p-tolyl)isoxazol-3-yl)methoxy)phenyl)methanimine (**7**): yield 75%, mp 117–118 °C; IR (KBr) ν 3122 (CH_{isox}), 2973, 2904, 2846, 1643 (C=N), 1605, 1581, 1510, 1474, 1451, 1342, 1251 (CH_2–O), 1169, 1048, 833, 821, 788 cm^{-1}; ^1H NMR ($CDCl_3$, 500 MHz) *δ* 1.12 (3H, d, *J* = 6.6 Hz, CH_3), 1.47–1.60 (6H, m, $3CH_2$), 1.61–1.75 (6H, m, $3CH_2$), 1.92–2.02 (3H, m, 3CH), 2.75 (1H, q, *J* = 6.5 Hz, CH_3CHN,), 5.22 (2H, s, CH_2–O), 6.59 (1H, s, CH_{isox}), 7.02 ($2H_{Ar}$, d, *J* = 8.7 Hz), 7.25 ($2H_{Ar}$, d, *J* = 8.3 Hz), 7.66 ($2H_{Ar}$, d, *J* = 8.1 Hz), 7.70 ($2H_{Ar}$, d, *J* = 8.7 Hz), 8.13 (1H, s, CH=N); ^{13}C NMR ($CDCl_3$, 125 MHz) *δ* 16.02 (CH_3), 21.65 (CH_3), 28.85 (3CH), 37.56 (3CH2), 39.34 (3CH2), 62.03 (CH_2–O), 76.12 (CH_3CHN), 98.31 (CH_{isox}), 114.87 ($2CH_{Ar}$), 125.97 ($2CH_{Ar}$), 129.82 ($2CH_{Ar}$), 129.83 ($2CH_{Ar}$), 157.75 (CH=N), 36.22, 124.66, 130.75, 140.84, 159.78, 161.31, 170.97 ($7C_{quater}$); MS *m*/*z* (I_{rel}, %) 455.20 $[M+H]^+$ (100); Anal. calcd. for $C_{30}H_{34}N_2O_2$ (454.61): C, 79.26; H, 7.54; N, 6.16%; Found: C, 79.38; H, 7.67; N, 6.02%.

N-(1-(adamantan-1-yl)ethyl)-1-(4-((4,5-dichloroisothiazol-3-yl)methoxy)-3-methoxyphenyl) methanimine (**8**): yield 72%, mp 93–95 °C; IR (KBr) ν 2963, 2902, 2844, 2802, 1646 (C=N), 1591, 1512, 1467, 1421, 1378, 1274 (CH_2–O), 1232, 1163, 1138, 1103, 1021, 979, 963, 869, 800, 754 cm^{-1}; ^1H NMR ($CDCl_3$, 500 MHz) *δ* 1.12 (3H, d, *J* = 6.6 Hz, CH_3), 1.49–1.60 (6H, m, $3CH_2$), 1.61–1.75 (6H, m, $3CH_2$), 1.90–2.02 (3H, m, 3CH), 2.75 (1H, q, J = 6.5 Hz, CH_3CHN), 3.93 ($1H_{Ar}$, s, *J* = 1.8 Hz), 8.09 (1H, s, CH=N); ^{13}C NMR ($CDCl_3$, 125 MHz) *δ* 16.02 (CH_3), 28.84 (3CH), 37.55 ($3CH_2$), 39.34 ($3CH_2$), 56.24 (OMe), 66.76 (CH_2–O), 76.13 (CH_3CHN), 110.44 ($1CH_{Ar}$), 114.21 ($1CH_{Ar}$), 122.19 ($1CH_{Ar}$), 157.94 (CH=N), 36.23, 123.25, 131.63, 148.65, 149.46, 150.25, 162.07 ($7C_{quater}$); MS *m*/*z* (I_{rel}, %) 480.1 $[M+H]^+$ (100); Anal. calcd. for $C_{24}H_{28}Cl_2N_2O_2S$ (479.46): C, 60.12; H, 5.89; Cl, 14.79; N, 5.84; S, 6.69%; Found: C, 60.25; H, 5.97; Cl, 14.69; N, 5.75; S, 6.61%.

4-(((1-(adamantan-1-yl)ethyl)imino)methyl)-2-methoxyphenyl adamantane-1-carboxylate (**9**): yield 68%, mp 198–199 °C; IR (KBr) ν 3075, 2958, 2933, 2904, 2849, 2659, 1753 (C=O), 1647 (C=N), 1601, 1504, 1464, 1452, 1417, 1381, 1360, 1346, 1323, 1273, 1249, 1216, 1195, 1182, 1154, 1121, 1102, 1093, 1078, 1050, 1044, 979, 960, 936, 899, 874, 816, 753, 729, 677, 619 cm^{-1}; ^1H NMR ($CDCl_3$, 500 MHz) *δ* 1.13 (3H, d, *J* = 6.6 Hz, CH_3CHN), 1.48–1.61 (6H, m, $3CH_2$), 1.61–1.74 (6H, m, $3CH_2$), 1.74–1.81 (6H, m, $3CH_2$), 1.95–2.00 (3H, m, 3CH), 2.06–2.11 (9H, m, $3CH_2$+3CH), 2.78 (1H, q, *J* = 6.6 Hz, CH_3CHN,), 3.87 (3H, s, OCH_3), 7.01 ($1H_{Ar}$, d, *J* = 8.0 Hz), 7.21 ($1H_{Ar}$, dd, *J* = 8.0, 1.7 Hz), 7.44 ($1H_{Ar}$, d, *J* = 1.7 Hz), 8.13 (1H, s, CH=N); ^{13}C NMR ($CDCl_3$, 125 MHz) *δ* 15.99 (CH_3CHN), 28.14 (3CH), 28.85 (3CH), 36.68 ($3CH_2$), 37.57 ($3CH_2$), 38.98 ($3CH_2$), 39.35 ($3CH_2$), 56.22 (OCH_3), 76.15 (CH_3CHN), 110.98 ($1CH_{Ar}$), 121.76 ($1CH_{Ar}$), 122.87 ($1CH_{Ar}$), 157.90 (CH=N), 36.25, 41.27, 135.56, 142.20, 151.60 175.75 (C=O) ($6C_{quater}$); MS *m*/*z* (I_{rel}, %) 476.30 $[M+H]^+$ (100); Anal. calcd. for $C_{31}H_{41}NO_3$ (475.66): C, 78.28; H, 8.69; N, 2.94%; Found: C, 78.52; H, 8.75; N, 2.83%.

General Procedure for the Synthesis of Amines **10**–**13**. To a suspension of 0.17 g (4.5 mmol) of $NaBH_4$ in 50 mL of anhydrous benzene, 0.81 g (13.5 mmol) of glacial acetic acid was added in portions and stirred for 30 min. Then, 1.5 mmol of imine was added. The mixture was stirred for 4 h, and then treated with 100 mL of water. Sodium hydrogen carbonate 3.8 g (45 mmol) was added in small portions and stirred for 1 h. The organic layer was washed with water and dried with sodium sulfate, before benzene was removed on a rotary evaporator and the residue was recrystallized from a benzene–hexane mixture.

1-(Adamantan-1-yl)-N-((5-phenylisoxazol-3-yl)methyl)ethan-1-amine (**10**): yield 68%, oil; IR (KBr) ν 3345 (N–H), 3063, 2902, 2847, 1615, 1592, 1574, 1451, 1423, 1377, 1155, 1100, 765, 690 cm^{-1}; ^1H NMR ($CDCl_3$, 500 MHz) δ 1.00 (3H, d, J = 6.5 Hz, CH_3), 1.44–1.51 (3H, m, $3CH_2$), 1.57–1.66 (6H, m, $3CH_2$), 1.67–1.73 (3H, m, $3CH_2$), 1.93–2.00 (3H, m, 3CH), 2.13 (1H, q, J = 6.5 Hz, CH_3CHNH), 3.80 (1H, d, J = 14.3 Hz, CH_2NH), 3.98 (1H, d, J = 14.3 Hz, CH_2NH), 6.54 ($1H_{isox}$, s), 7.39–7.49 ($3H_{Ar}$, m), 7.75–7.80 ($2H_{Ar}$, m); ^{13}C NMR ($CDCl_3$, 125 MHz) δ 13.37 (CH_3), 28.70 (3CH), 37.47 ($3CH_2$), 38.76 ($3CH_2$), 43.82 (CH_2NH), 61.70 (CH_3CHNH), 99.28 (CH_{isox}), 125.95 ($2CH_{Ar}$), 129.08 ($2CH_{Ar}$), 130.17 ($1CH_{Ar}$), 36.30, 127.80, 164.47, 169.79 ($4C_{quater}$); MS m/z (I_{rel}, %) 337.30 $[M+H]^+$ (100); Anal. calcd. for $C_{22}H_{28}N_2O$ (336.48): C, 78.53; H, 8.39; N, 8.33%; Found: C 78.65; H 8.47; N 8.09%.

1-(Adamantan-1-yl)-N-((5-(p-tolyl)isoxazol-3-yl)methyl)ethan-1-amine (**11**): yield 69%, oil; IR (KBr) ν 3346 (N–H), 3138, 3033, 2904, 2846, 1619, 1598, 1514, 1465, 1451, 1432, 1377, 1344, 1315, 1184, 1154, 1113, 1103, 1045, 948, 822, 799, 505 cm^{-1}; ^1H NMR ($CDCl_3$, 500 MHz) δ 1.00 (3H, d, J = 6.5 Hz, CH_3), 1.44–1.51 (3H, m, $3CH_2$), 1.59–1.65 (6H, m, $3CH_2$), 1.66–1.73 (3H, m, $3CH_2$), 1.94–1.99 (3H, m, 3CH), 2.13 (1H, q, J = 6.5 Hz, CH_3CHNH), 2.39 (3H, s, CH_3), 3.79 (1H, d, J = 14.3 Hz, CH_2NH), 3.97 (1H, d, J = 14.3 Hz, CH_2NH), 6.48 ($1H_{isox}$, s), 7.25 ($2H_{Ar}$, d, J = 8.1 Hz), 7.66 ($2H_{Ar}$, d, J = 8.1 Hz); ^{13}C NMR ($CDCl_3$, 125 MHz) δ 13.37 (CH_3), 21.62 (CH_3), 28.71 (3CH), 37.47 ($3CH_2$), 38.76 ($3CH_2$), 43.85 (CH_2NH), 61.71 (CH_3CHNH), 98.67 (CH_{isox}), 125.90 ($2CH_{Ar}$), 129.76 ($2CH_{Ar}$), 36.30, 125.11, 140.42, 164.39, 169.98 ($5C_{quater}$); MS m/z (I_{rel}, %) 351.30 $[M+H]^+$ (100); Anal. calcd. for $C_{23}H_{30}N_2O$ (350.51): C, 78.82; H, 8.63; N, 7.99%; Found: C, 78.96; H, 8.75; N, 7.82%.

1-(Adamantane-1-yl)-N-((5-(4-nitrophenyl)isoxazol-3-yl)methyl)ethan-1-amine (**12**): yield 75%, mp 85–87 °C; IR (KBr) ν 3380, 3267 (N–H); 3129, 2903, 2846, 1605, 1582, 1519 (N–O), 1449, 1425, 1348 (N–O), 1313, 1157, 1106, 1047, 1010, 947, 853, 813, 754, 692 cm^{-1}; ^1H NMR (DMSO-d6, 500 MHz) δ 0.89 (3H, d, J = 6.5 Hz, CH_3), 1.34–1.42 (3H, m, $3CH_2$), 1.51–1.58 (6H, m, $3CH_2$), 1.58–1.65 (3H, m, $3CH_2$), 1.85–1.91 (3H, m, 3CH), 1.95 (1H, q, J = 6.5 Hz, CH_3CHNH), 3.70 (1H, d, J = 14.5 Hz, CH_2NH), 3.87 (1H, d, J = 14.5 Hz, CH_2NH), 7.24 ($1H_{isox}$, s), 8.08–8.12 ($2H_{Ar}$, m), 8.30–8.36 ($2H_{Ar}$, m); ^{13}C NMR (DMSO-d6, 125 MHz) δ 13.37 (CH_3), 28.55 (3CH), 37.44 ($3CH_2$), 38.65 ($3CH_2$), 43.36 (CH_2NH), 61.22 (CH_3CHNH), 103.59 (CH_{isox}), 125.01 ($2CH_{Ar}$), 127.25 ($2CH_{Ar}$), 36.37, 133.07, 148.47, 165.66, 166.78 ($5C_{quater}$); Anal. calcd. for $C_{22}H_{27}N_3O_3$ (381.48): C, 69.27; H, 7.13; N, 11.02%; Found: C, 69.38; H, 7.25; N, 10.82%.

1-(Adamantan-1-yl)-N-(4-((5-(p-tolyl)isoxazol-3-yl)methoxy)benzyl)ethan-1-amine (**13**): yield 95%, mp 89–90 °C; IR (KBr) ν 3422 (N–H), 3139 (CH_{isox}), 3059, 3033, 2903, 2845, 1617, 1600, 1586, 1507, 1466, 1449, 1365, 1299, 1232 (CH_2–O), 1168, 1120, 1044, 1023, 947, 857, 810, 782, 504 cm^{-1}; ^1H NMR ($CDCl_3$, 500 MHz) δ 0.97 (3H, d, J = 6.5 Hz, CH_3), 1.40–1.50 (3H, m, $3CH_2$), 1.55–1.65 (6H, m, $3CH_2$), 1.66–1.74 (3H, m, $3CH_2$), 1.90–1.99 (3H, m, 3CH), 2.09 (1H, q, J = 6.5 Hz, CH_3CHN), 2.40 (3H, s, CH_3), 3.58 (1H, d, J = 13.1 Hz, CH_2), 3.86 (1H, d, J = 13.1 Hz, CH_2), 5.18 (2H, s, CH_2–O), 6.59 ($1H_{isox}$, s), 6.96 ($2H_{Ar}$, d, J = 8.6 Hz), 7.22–7.30 ($4H_{Ar}$, m), 7.66 ($2H_{Ar}$, d, J = 8.2 Hz); ^{13}C NMR ($CDCl_3$, 125 MHz) δ 13.42 (CH_3), 21.65 (CH_3), 28.76 (3CH), 37.53 ($3CH_2$), 38.85 ($3CH_2$), 52.14 (CH_2–NH), 61.50 (CH_3CHNH), 62.07 (CH_2–O), 98.39 (CH_{isox}), 114.70 ($2CH_{Ar}$), 125.96 ($2CH_{Ar}$), 129.60 ($2CH_{Ar}$), 129.82 ($2CH_{Ar}$), 36.32, 124.73, 134.56, 140.75, 157.13, 161.67, 170.81 ($7C_{quater}$); MS m/z (I_{rel}, %) 457.20 $[M+H]^+$

(100); Anal. calcd. for $C_{30}H_{36}N_2O_2$ (456.63): C, 78.91; H, 7.95; N, 6.13%; Found: C, 79.12; H, 8.06; N, 6.01%.

The general procedure for the synthesis of amidoesters **14**, **16** and amidoether **15** is given in [34].

4-((N-(1-Adamantan-1-yl)ethyl)-4,5-dichloroisothiazole-3-carboxamido)methyl)phenyl 4,5-dichloroisothiazole-3-carboxylate (**14**): yield 74%, mp 135–136 °C; IR (KBr) ν 2979, 2918, 2900, 2850, 1743 (C=O), 1647 (C=O), 1505, 1471, 1453, 1352, 1321, 1275, 1211, 1184, 1172, 1070, 964, 830, 745, 683, 509 cm^{-1}; ^1H NMR (DMSO-d6, 500 MHz) δ 1.22, 1.28 (3H, d, J = 7.2 Hz, CH_3); 1.41–1.50 (3H, m, $3CH_2$); 1.50–1.64 (3H, m, $3CH_2$); 1.65–1.74 (6H, m, $3CH_2$); 1.89–2.20 (3H, m, 3CH); 3.53, 4.63 (1H, q, J = 7.0 Hz, CH_3CHN); 4.47, 4.57 (1H, d, J = 16.6 Hz, CH_2N); 4.74, 4.98 (1H, d, J = 16.6 Hz, CH_2NH); 7.09, 7.13 ($2H_{Ar}$, d, J = 8.6 Hz); 7.27, 7.45 ($2H_{Ar}$, d, J = 8.6 Hz); ^{13}C NMR (DMSO-d6, 125 MHz) δ 11.83, 13.31 (CH_3CHN); 28.47 (3CH); 36.76, 37.05 ($3CH_2$), 39.36, 39.51 ($3CH_2$); 47.15, 49.01 (CH_2N), 57.56, 63.91 (CH_3CHN), 121.83, 121.97 ($2CH_{Ar}$); 127.91, 128.42 ($2CH_{Ar}$); 37.74, 38.50; 122.15, 122.46; 125.71; 137.10, 137.44; 148.38, 148.95; 149.13, 149.73; 151.17, 151.21; 153.15, 153.24; 157.38, 157.62; 160.98; 163.76, 163.79 ($11C_{quater}$); MS m/z (I_{rel}, %) 646.00 $[M+H]^+$ (100); Anal. calcd. for $C_{27}H_{25}C_{l4}N_3O_3S_2$ (645.44): C, 50.24; H, 3.90; Cl, 21.97; N, 6.51; S, 9.93%; Found: C, 50.39; H, 3.98; Cl, 21.84; N, 6.41; S, 9.85%.

*N-(1-Adamantan-1-yl)ethyl)-4,5-dichloro-N-(4-((4,5-dichloroisothiazol-3-yl)methoxy)-3-*methoxybenzyl)isothiazole-3-carboxamide (**15**): yield 76%, mp 139–140 °C; IR (KBr) ν 3067, 2902, 2847, 1645 (C=O), 1606, 1593, 1511, 1449, 1417, 1377, 1353, 1317, 1262, 1220, 1177, 1140, 1031, 971, 945, 808, 733, 710, 672 cm^{-1}; MS m/z (I_{rel}, %) 661.00 $[M+H]^+$ (100); Anal. calcd. for C28H29Cl4N3O3S2 (661.48): C, 50.84; H, 4.42; Cl, 21.44; N, 6.35; S, 9.69%; Found: C, 50.98; H, 4.58; Cl, 21.31; N, 6.24; S, 9.57%.

3-((N-(1-Adamantan-1-yl)ethyl)-5-(p-tolyl)isoxazole-3-carboxamido)methyl)phenyl 5-(p-tolyl) isoxazole-3-carboxylate (**16**): yield 74%, mp 163–165 °C; IR (KBr) ν 3142, 3125, 2992, 2900, 2846, 1750 (C=O), 1627 (C=O), 1613, 1593, 1509, 1475, 1440, 1412, 1390, 1330, 1225, 1201, 1143, 1103, 991, 959, 948, 806, 767, 749, 678, 501 cm^{-1}; ^1H NMR ($CDCl_3$, 500 MHz) δ 1.22, 1.31 (3H, d, J = 7.0 Hz, CH_3); 1.51–1.59 (3H, m, $3CH_2$); 1.60–1.68 (3H, m, $3CH_2$); 1.68–1.77 (6H, m, 3CH2); 1.95–2.07 (3H, m, 3CH); 2.36, 2.40 (3H, s, $CH_{3\ p\text{-}Tol}$); 2.42, 2.43 (3H, s, $CH_{3\ p\text{-}Tol}$); 4.43, 4.58 (1H, d, J = 17.0 Hz, CH_2N); 4.58, 4.87 (1H, q, J = 7.2 Hz, CH_3CHN); 5.19, 5.38 (1H, d, J = 17.0 Hz, CH_2NH); 6.41, 6.78 ($1H_{isox}$, s), 6.95, 6.98 ($1H_{isox}$, s); 6.96–7.05, 7.12–7.16 ($2H_{Ar}$, m); 7.19–7.41 ($6H_{Ar}$, m), 7.53, 7.70 ($2H_{Ar}$, d, J = 8.1 Hz); 7.71–7.74 ($2H_{Ar}$, m); ^{13}C NMR ($CDCl_3$, 125 MHz) δ 11.62, 13.15 (CH_3CHN); 21.62, 21.66 (CH_3); 21.69 (CH_3); 28.89, 28.67 (3CH); 36.87, 37.08 ($3CH_2$), 39.53, 39.78 ($3CH_2$); 47.90, 49.37 (CH_2N); 57.90, 63.01 (CH_3CHN); 99.81, 100.52 (CH_{isox}); 99.82, 99.84 (CH_{isox}); 119.60, 119.88 ($1CH_{Ar}$); 119.91, 119.95 ($1CH_{Ar}$); 124.79, 124.96 ($1CH_{Ar}$); 126.01, 126.04 ($2CH_{Ar}$); 126.08 ($2CH_{Ar}$); 129.73, 129.90 ($2CH_{Ar}$); 129.78 ($1CH_{Ar}$); 130.01, 130.04 ($2CH_{Ar}$); 38.46, 38.68; 123.93, 124.00; 124.30; 140.46, 140.74; 141.09, 141.52; 141.62, 146.68; 150.37, 150.46; 156.45, 156.63; 158.56; 160.08, 160.51; 162.97, 163.77; 169.89, 170.56; 172.43, 172.53 ($13C_{quater}$); MS m/z (I_{rel}, %) 656.30 $[M+H]^+$ (71.5); Anal. calcd. for $C_{41}H_{41}N_3O_5$ (655.80): C, 75.09; H, 6.30; N, 6.41%; Found: C, 75.21; H, 6.45; N, 6.32%.

2.2. Biology

The cytotoxicity and antiviral activity of the synthesized amides against the vaccinia virus were evaluated using a colorimetric assay in Vero cell cultures [35]. The vaccinia virus (strain Copenhagen) obtained from the State collection of pathogens of viral infections and rickettsioses of the SRC VB Vector (Koltsovo, Novosibirsk region, Russia) were used in this work. The virus was propagated in Vero cells in DMEM (BioloT, Russia). The concentration of the virus in the cell culture supernatant was determined by plaque assay

titration, calculated, and expressed as decimal logarithms of plaque-forming units per milliliter (log_{10} PFU per ml). The viruses used in this experiment had a titer between 5.6 and 6.1 log_{10} PFU/mL. The stock of these viruses was stored at −70 °C. The commercially available drug Cidofovir (Cidofovir, Vistide) manufactured by Gilead Sciences Inc. was used as a reference (Foster City, CA, USA). To evaluate the antiviral activity, firstly, a 50 µL dilution of samples was added to the wells of 96-well plates with a monolayer of cells containing 100 µL of DMEM medium with 2% fetal serum, and then 50 µL of a 1000 PFU per well virus dose was added. The cytotoxicity of the compounds was determined by measuring cell destruction under the influence of wells that did not contain any virus. Cell monolayers in plate wells were used as controls: the virus was added to one set of wells (virus control), and the other set contained neither the virus nor any compound (cell culture control). After incubating cell monolayers infected with orthopoxvirus for 4 days and treating them with the compounds being tested, a vital dye, "neutral red", was added to the culture medium for 1.5 h. Next, the monolayer was washed twice with saline solution, the lysis buffer was added and, after 30 min, the optical density (OD), which is an indicator of the number of cells in the monolayer not destroyed in the presence of the virus, was measured on an Emax plate reader (Molecular Devices, San Jose, CA, USA) at 490 nm. The OD values were used to calculate a 50% cytotoxic concentration (CC_{50} µM) and a 50% virus inhibiting concentration (EC_{50} µM) using the SoftMax Pro-4.0 computer program. Based on these indicators, the selectivity index (SI) was calculated: $SI = CC_{50}/EC_{50}$.

2.3. Molecular Modeling

All theoretical calculations were carried out using software Schrodinger release 2020-2 [Schrodinger, M. Small Molecule Drug Discovery Suite; Schrödinger LLC: New York, NY, USA, 2020]. The geometrical parameters of the ligands were optimized using OPLS4 force field [36], considering all possible conformations.

2.3.1. The Pharmacophore Model

The creation of pharmacophore profiles for tecovirimat and the generation of conformers for compounds **1**–**16**, as well as the comparison of their pharmacophores, were performed in Phase, using the plugin Develop Pharmacophore Hypotheses. The pharmacophore model is based on tecovirimat and it contains eight pharmacophoric centers. Molecules **1**–**16** were tested for compatibility with the pharmacophore profile of tecovirimat, and compounds **1**, **2**, **4**, **5**, **7**, and **12** were selected as active. Based on biological testing, these molecules showed antiviral activity against VACV (Copenhagen strain). Fifty conformations of each molecule were generated, and their pharmacophore profiles were checked against the pharmacophore model of tecovirimat.

2.3.2. Molecular Docking

The geometric parameters of ligands 1, 2, 4, 5, 7, 10, 12 are optimized in the force field OPLS4 [27] using the LigPrep plugin. The possibility of the existence of protonated forms of the ligands was tested using the Epik plugin [37] at pH = 7 ± 2. These ligands inhibit the VACV strain (Copenhagen strain) according to the in vitro test. For compounds **5**, **7**, **10** and **12** the calculations were performed for the R- and S-stereoisomers, as these compounds represent the mixtures of stereoisomeric forms. The tertiary structure of the p37, determined using the ColabFold methodology [38] and described in [28,29] (File S1), was used in the calculations. The region of the phospholipase domain described in the work [28] was considered to be a binding site for potential inhibitors of the p37 protein. Model structures were prepared using plugin Protein PrepWizard: hydrogen atoms were added and minimized, side chains of amino acids were edited, the multiplicity of chemical

bonds was restored, and water molecules were removed. Geometric parameters were optimized in the OPLS4 force field and converge heavy atoms to RMSD 0.3 Å.

Molecular docking was performed using the protocol of forced ligand positioning (IFD) with the following conditions: a flexible protein and a ligand was used, a grid matrix size of 15 Å was used, amino acids within a radius of 5 Å from the ligand were optimized taking into account the influence of the ligand, and SP precision was ensured. The maximum number of ligand poses was limited to 20. The ranking of the docking solutions was carried out based on the evaluation of the following calculated parameters: docking score, energy model value (E_{model}), and visualization of the ligand location in the binding site. Based on these parameters, an optimal position was chosen to calculate the Gibbs energy of protein binding and perform molecular dynamic calculations. Gibbs binding energy (ΔG_{bind}) was calculated using Prime MM-GBSA under the conditions of solvation model VSGB, flexible protein, and a ligand with amino acids within a radius of 5 Å from the ligand, optimized considering the influence of the ligand. The docking position was selected based on a combination of energy parameters, including the docking score, the energy model value (Emodel), the visualization of the ligand position in the binding site, and the absence of clash interactions.

2.3.3. Molecular Dynamics

Molecular dynamics simulations were performed on the ligand–protein complex of compound **2** bound to p37. The complex was placed in an orthorhombic box with buffer space of 20 Å, and the box was filled with an aqueous solution of 0.15 M NaCl. The water model was TIP3P, and Na^+ counterions were added to equalize the charges of the system. All models underwent a relaxation procedure of 2 ns to minimize internal stresses before the simulation time of 150 ns and 1000 analyzed frames. The thermodynamic ensemble was NPT.

2.4. Single-Crystal X-Ray Diffraction

For additional characterization of the obtained compounds and confirmation of their isomerism, studies were carried out on single crystals of these compounds. Single crystals of compounds **5** and **7** that were suitable for crystallographic analysis and structure determination were grown from saturated solutions of these compounds in DMF using the slow evaporation technique. Single-crystal X-ray diffraction data were collected at 296(2) K using a TD-5000 diffractometer with Mo-Kα radiation (λ = 0.71073 Å), equipped with a hybrid photon-counting detector (Table S1). The obtained diffraction data were converted into a standard ESPERANTO format [39]. Data reduction, scaling, and absorption correction were carried out using the CrysAlis PRO program package (v. 1.171.42.49) [40]. Structure was determined, and refinement was performed, using SHELXT [41] and SHELXL [42] programs with Olex2 (v. 1.5) as a GUI [43]. All non-hydrogen atoms were refined anisotropically. The positions of hydrogen atoms were treated using constrained refinement using a riding model [U_{iso} (H) = 1.2 U_{eq} (C)]. Structure validation was carried out using CheckCIF service [44]. For the visualization of crystal structures, the Mercury software (v. 2022.1.0) was used [45].

CCDC 2412919 and 2412920 contain the supplementary crystallographic data for this paper. These data can be obtained free of charge from The Cambridge Crystallographic Data Centre via https://www.ccdc.cam.ac.uk (accessed on 25 December 2024).

3. Results

3.1. Chemistry

Based on the literature data showing that adamantane derivatives can exhibit significant activity against orthopoxviruses, in the present work, a library of compounds contain-

ing an adamantane fragment was synthesized in order to study their anti-orthopoxviral properties. Specifically, compounds **1**–**4** were synthesized based on 1-adamantane amine using the previously described methodology (Scheme 1).

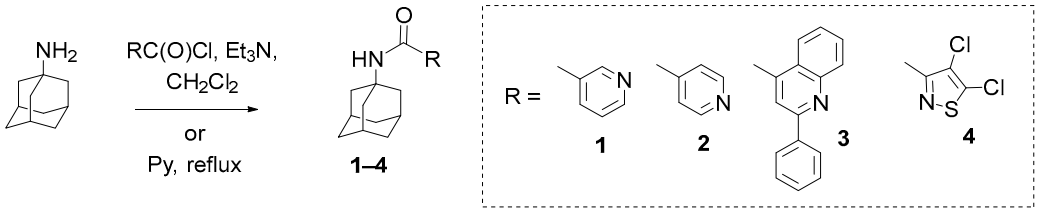

Scheme 1. Synthesis of compounds **1**–**4** from 1-adamantane amine.

The synthesis of compounds **1** and **2** was described in [46], and the synthesis of derivative **3** containing 2-phenylquinoline-4-carboxamide fragment was described in [47], but a physicochemical description of compounds **1**–**3** was not previously provided. Compound **4** has not been described before in the literature.

In order to identify which structural blocks are important for the biological activity, a library of compounds was synthesized on the basis of 1-adamantane carboxylic acid according to the methodology developed earlier [34]. In particular, imines **5**–**9** were obtained in one step from rimantadine and corresponding aldehydes, compounds **10**–**16** were synthesized through a reduction in the imino group and further acylation of the compounds with active amino and hydroxyl groups yielded amidoethers **14**–**16,** which were found to be a mixture of isomers (Scheme 2). The synthesized adamantane derivatives have pharmacophore 1,2-azole fragments linked directly to the rimantadine fragment or through a hydroxybenzaldehyde linker.

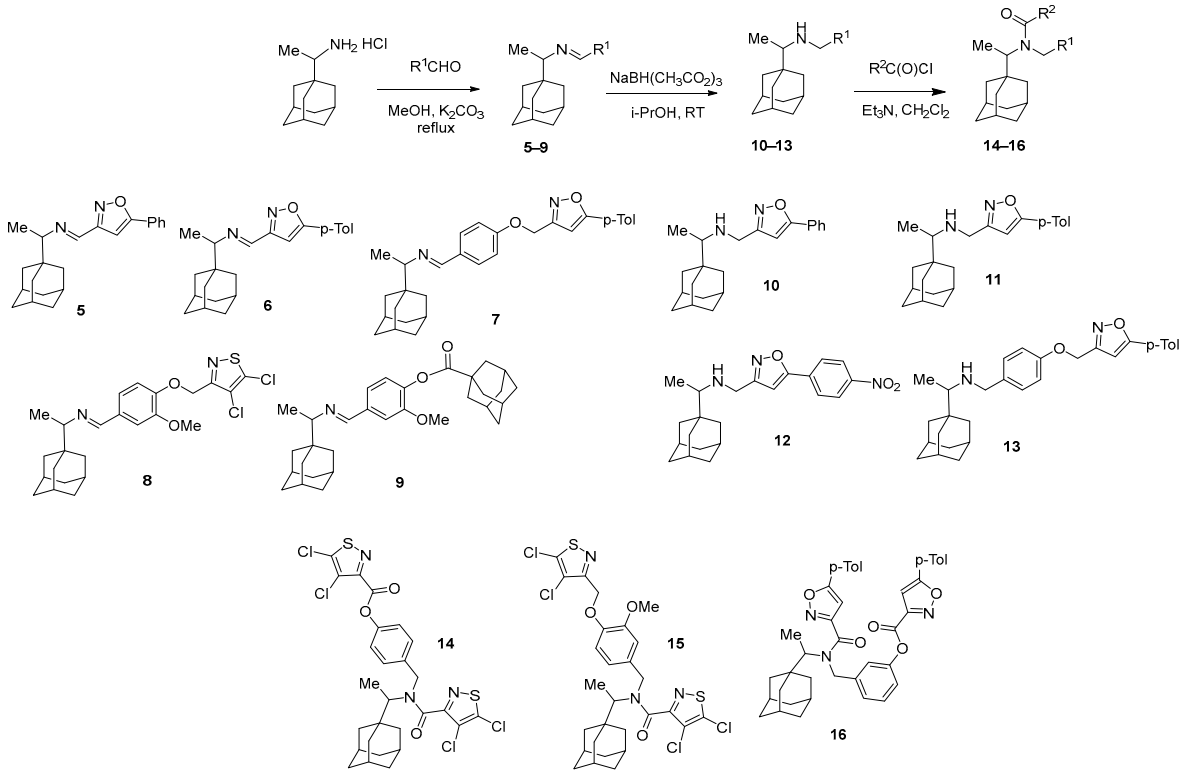

Scheme 2. Synthesis of adamantane derivatives **5**–**16** from rimantadine.

3.2. Crystal Structure Analysis

Compounds **5** and **7** crystallized in the monoclinic space group $P2_1/c$, with four molecules per unit cell (one molecule in the asymmetric unit). The molecules of **5** and **7** in

the crystalline state exist in the form of E-isomers relative to the N1=C13 bond in the imine fragment (Figure S1).

No hydrogen bonds are present in the crystal structures of both compounds **5** and **7** due to the lack of suitable H-atom donors. The crystal packing of **5** contains pairs of antiparallel-displaced molecules linked by medium-strength π···π stacking interactions between the isoxazole rings (the distance between the centroids of these rings is 3.38 Å; Figure 2). Short intermolecular contacts between hydrogen atoms H5 (atom numbering scheme presented herein, in accordance with that in the corresponding CIFs) belonging to adamantane fragments of neighboring molecules were also observed in the structure (H···H distance is 2.36 Å).

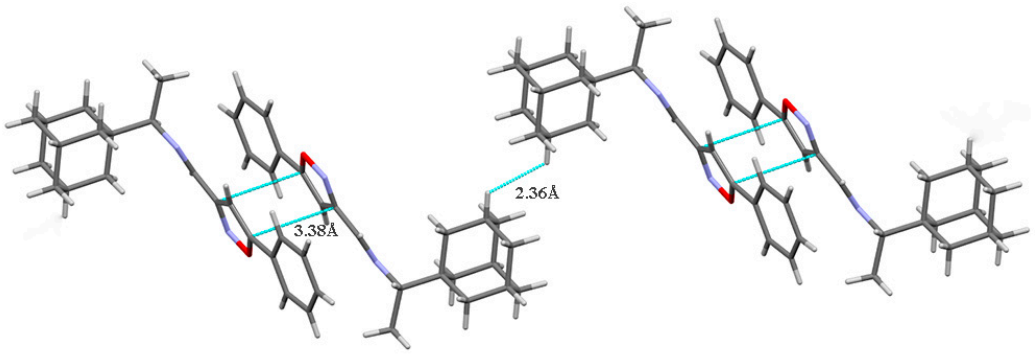

Figure 2. The crystal packing of compound **5**. Dashed lines indicate stacking interactions and short intermolecular contacts.

The crystal structure of **7** consists of layers containing antiparallel-displaced molecules (Figure 3a). Due to the displacement of neighboring molecules in the adjacent layers, no medium-strength or strong stacking interactions were present in the crystal packing. However, several short intermolecular contacts can be distinguished in the structure: the shortest ones are observed between the heteroatoms of isoxazole ring and hydrogen atoms of the acyclic methylene group (N2 and H20A atoms at a distance of 2.74 Å, Figure 3b; O2 and H20B atoms at a distance of 2.61 Å, Figure 3c) and between the carbon and hydrogen atoms of neighboring phenyl moieties (C28 and H28 atoms at a distance of 2.88 Å, Figure 3d).

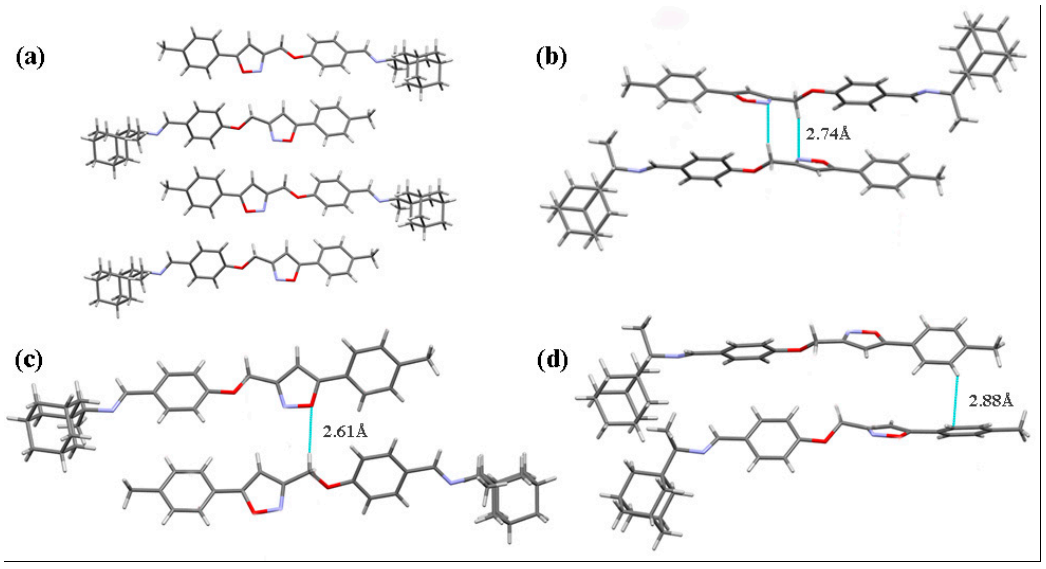

Figure 3. The views of crystal packing of compound **7** showing the set of molecular layers (**a**) and short intermolecular contacts (**b**–**d**). Dashed lines indicate short intermolecular contacts.

3.3. Biology

The activity of the obtained compounds against orthopoxviruses was investigated using vaccinia viruses (Copenhagen strain); the values of inhibitory activity (EC_{50}) and cytotoxicity (CC_{50}) were evaluated using an adapted colorimetric method in Vero cell culture [35] (Table 1). Cidofovir (Heritage Consumer Products, LLC, East Brunswick, NJ, USA) was used as a positive control. Our results on the activity of Cidofovir correlate with the previously published data [15].

Table 1. CC_{50}, EC_{50}, and SI values for **1–16**. Compounds exhibiting the highest SI values are highlighted in green.

Compound	CC_{50}, μM [a]	EC_{50}, μM [b]	SI [c]
1	100.67 ± 21.1	16.78 ± 3.7	6
2	390.33 ± 26.1	3.45 ± 0.9	115
3	350.31 ± 38.9	NA	-
4	75.50 ± 8.7	2.91 ± 0.15	26
5	299.40 ± 41.0	75.53 ± 8.1	4
6	287.35 ± 11.7	NA	-
7	66.08 ± 5.1	40.8 ± 3.8	2
8	52.31 ± 2.5	NA	-
9	56.85 ± 2.7	NA [d]	-
10	15.47± 0.7	13.91 ± 2.5	-
11	15.14 ± 1.1	NA	-
12	204.72 ± 10.8	9.44 ± 1.5	22
13	10.47 ± 2.1	NA	-
14	8.87 ± 0.7	NA	-
15	21.31 ± 1.3	NA	-
16	150.37 ± 11.1	NA	-
Cidofovir	201.33 ± 60.10	7.63 ± 3.15	26

[a] CC_{50}—50% cytotoxic concentration at which 50% of cells in an uninfected monolayer are destroyed; [b] EC_{50}—50% virus-inhibiting concentration at which 50% of cells in the infected monolayer are not destroyed (retain viability); [c] SI—selectivity index; SI = CC_{50}/EC_{50}; [d] NA—not active; CC_{50} and EC_{50} values are presented as M ± SD, where M is the mean value and SD is the standard deviation with the number of CC_{50} and EC_{50} measurements $n = 3$.

As can be seen in Table 1, compounds **1–4,** based on 1-aminoadamantane, are not toxic to the investigated Vero cell line. Among imino derivatives **5–9,** based on rimantadine, compounds **5** and **6** are also not toxic, while the introduction of an additional methoxy–aromatic fragment into the structures of agents **7–9** significantly increased the toxic properties of the compounds. Among compounds **10–13**, agent **12,** containing a p-nitro substituent in the aromatic fragment and separated from the adamantane unit by an isoxazole linker, exhibits the least toxic properties. Among amidoethers **14–16**, agent **16** exhibits the lowest toxic properties. Compounds **2** and **4** show the highest activity in the lower micromolar range against vaccinia virus. At the same time, since compound **2** is much less toxic, its selectivity index is much higher and amounts to 115. Antiviral activity was also observed in compounds **1**, **10** and **12**. In general, it can be concluded that the most promising compounds for further studies are compounds **1**, **2**, **4** and **12**, among which the leading compound in this library is agent **2,** containing the isonicotine fragment.

3.4. Molecular Modeling Study

According to [27,28], compounds containing the adamantane fragment exhibit antiviral activity against orthopoxviruses by inhibiting the activity of the membrane viral protein p37. This suggests that the compounds studied in this work may also affect the function of the p37 protein. For this reason, molecular dockings of **1**, **2**, **4**, **5**, **7**, **10** and **12** were performed on the binding site of tecovirimat, a well-known p37 inhibitor.

The tecovirimat molecule contains a rigid hydrophobic fragment, donor–acceptor regions, an aromatic ring, and a hydrophobic $–CF_3$ group. The distance between the terminal carbon atoms is more than 14 Å (Figure 4a). The donor fragment of the molecule is surrounded by acceptors at a distance of about 3.5 Å. Tecovirimat binds to the region of the phospholipase domain of membrane protein p37, which is close to the phospholipase motif H(N)KD. This motif contains two key amino acid residues, Asn312 and Lys314, with which tecovirimat forms hydrogen bonds (Figure 4b). The tecovirimat carbon cell is surrounded by hydrophobic amino acid residues, such as leucine, cysteine, phenylalanine, and alanine. According to the results of molecular modeling [48], the binding energy of tecovirimat at the p37 binding site is -48 kcal/mol. In this case, the following pharmacophoric features should alternate in the structures of potential p37 protein inhibitors: a hydrophobic carbon cage (for example, an adamantane fragment [27,28]), a donor–acceptor group, an aromatic ring, and a hydrophobic substituent at the para position.

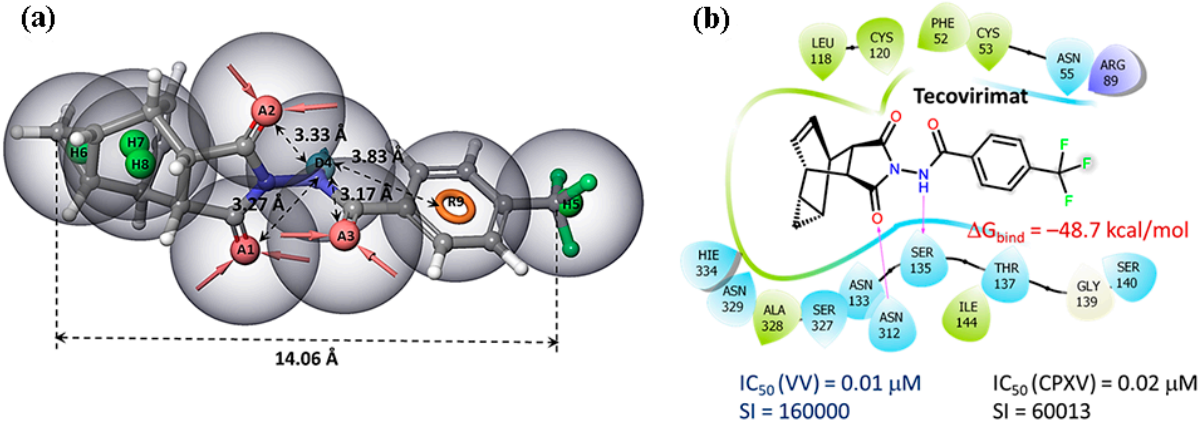

Figure 4. Pharmacophore analysis: (**a**) the pharmacophore profile of tecovirimat; (**b**) the location of tecovirimat at the p37 binding site according to the results of molecular modeling [48].

The pharmacophore profiles of molecules **1**–**16** were compared with the pharmacophore profile of tecovirimat. Among the studied compounds, only molecules **1**, **2**, **11S,** and **12S** had more than two coincidental pharmacophore features in relation to the tecovirimat pharmacophoric model. According to PhaseScreenScore (Table S2), which considers the number of matching features and their co-delivery quality, the profiles of compounds **1** and **2** come closest to that of tecovirimat, with compound **2** being the leader based on biological tests.

The pharmacophore profiles of agents **1** and **2** consist of a carbon hydrophobic cage containing donor–acceptor fragments and a pyridine ring (Figure 5a,b). The key similarity is the overlap of -NH-C=O fragments in compounds **1** and **2** and tecovirimat (Figure 5a,b). A π-π conjugate system is located ca. 4 Å away from this fragment, coinciding with the position of the aromatic ring of tecovirimat. The hydrophobic "cage" of adamantane is displaced by 1 Å. The PhaseScreenScore values for both compounds are commensurate and equal to 1.71.

Compound **11S** (Figure 5c) contains an acceptor and an aromatic fragment. The position of this fragment coincides with that of the acceptor A3 and aromatic fragment R9 in the pharmacophore model of tecovirimat, as well as with a hydrophobic group located at a distance of approximately 0.7 Å from the hydrophobic groups H6 and H7 in this model. The PhaseScreenScore for compound **11S** is 1.59.

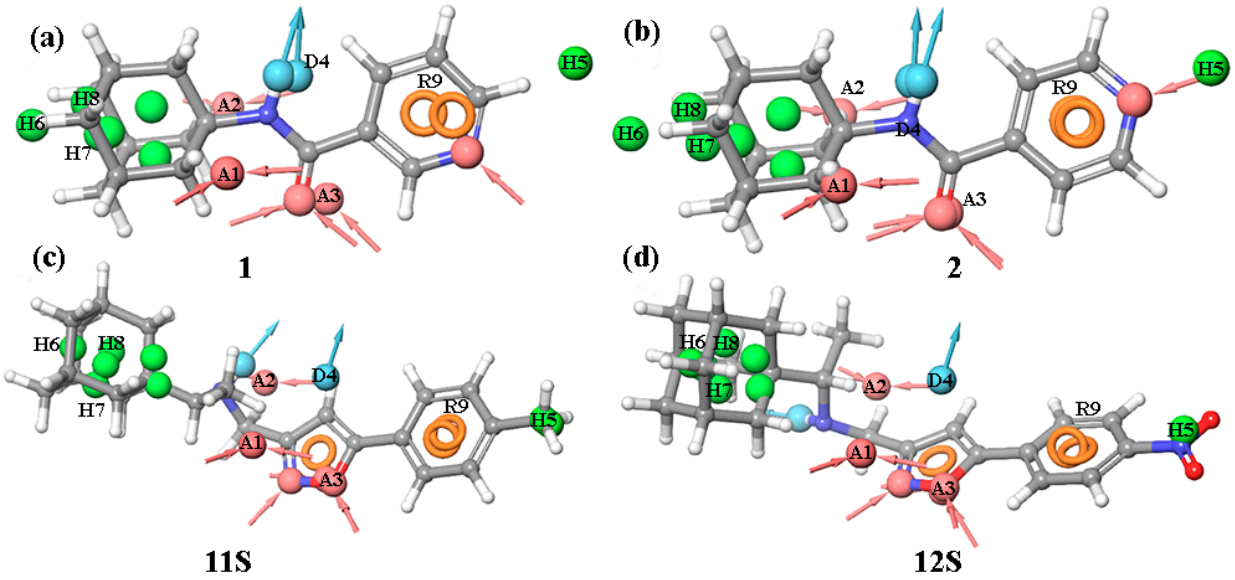

Figure 5. Pharmacophore analysis: the pharmacophore profiles of compounds **1** (**a**), **2** (**b**), **11S** (**c**) and **12S** (**d**) were compared with the pharmacophore model of tecovirimat.

Compound **12S** (Figure 5d) also has an acceptor group and an aromatic group. The location of these groups coincides with those of A3, R9, and H6-H8 in the tecovirimat pharmacophore. The $-NO_2$ group is located near H5 in the model, which makes it an acceptor. The PhaseScreenScore value for **12S** is 1.36. For **12R**, no more than two matching pharmacophoric features were obtained.

The pharmacophore analysis allows us to conclude that compounds **1**, **2** and **12S**, which are active against VACV (Copenhagen strain), have a pharmacophore profile similar to tecovirimat, what means that these compounds can be considered potential inhibitors of the phospholipase activity of membrane protein p37.

The molecular docking procedure was performed on the compounds that showed inhibitory activity against VACV (Copenhagen strain), according to the results of the biological testing (Table S2). Compounds **1**, **2**, **4**, **5R**, **5S**, **7R**, **7S**, **10R**, **10S**, **12R** and **12S** are located in the phospholipase region of the protein, containing amino acid residues Phe52, Leu118, Cys120, Ser135, Asn312, Lys314, and Asn329. When the leader, compound **2,** is located at the binding site (Figure 6a,b), the oxygen atom of the carbonyl group is connected to Lys314 by a hydrogen bond, while the nitrogen atom of the pyridine group is connected via an aqueous bridge with Lys281. Hydrophobic interactions were also observed with Asn329, Ala328, Phe52, and Ser135 (Figure 6c).

In the series of compounds **1**, **4**, **2**, **10S**, **10R**, a decrease in the Gibbs binding energy (ΔG_{bind}) was observed with a decrease in pIC_{50} values. The correlation index of pIC_{50} and ΔG_{bind} values was 0.5 (Figure 7). On the one hand, the correlation index value is low. However, it should be noted that we compared the values of the binding energy of ligands to the viral protein p37 binding site with the IC_{50} value, the semi-maximal concentration of the inhibition of the replication of infectious virus. One should not expect a high correlation index here, since the replication of viruses is a complex biological process involving both viral and cellular proteins. For this reason, we believe that the observed dependence may already indicate that the mechanism of the antiviral activity of the studied compounds is related to their effect on the function of p37.

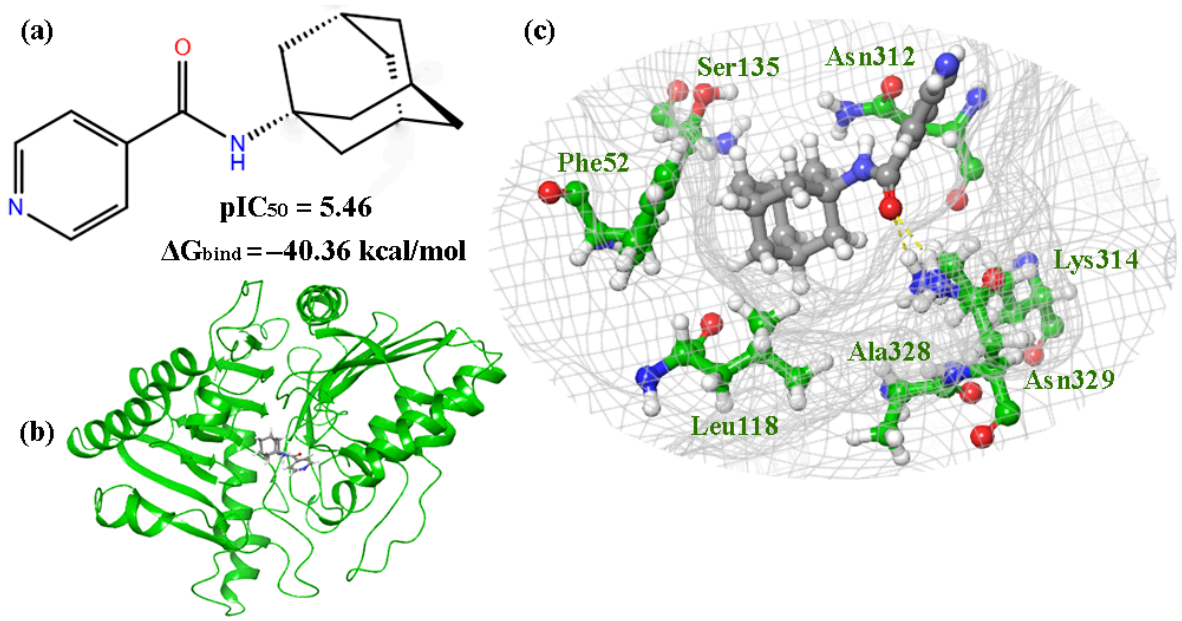

Figure 6. The results of molecular docking for compound **2**: (**a**) structures of lead compound **2**; (**b**) complex **2-p37**; (**c**) the location of compound **2** in the binding site of p37.

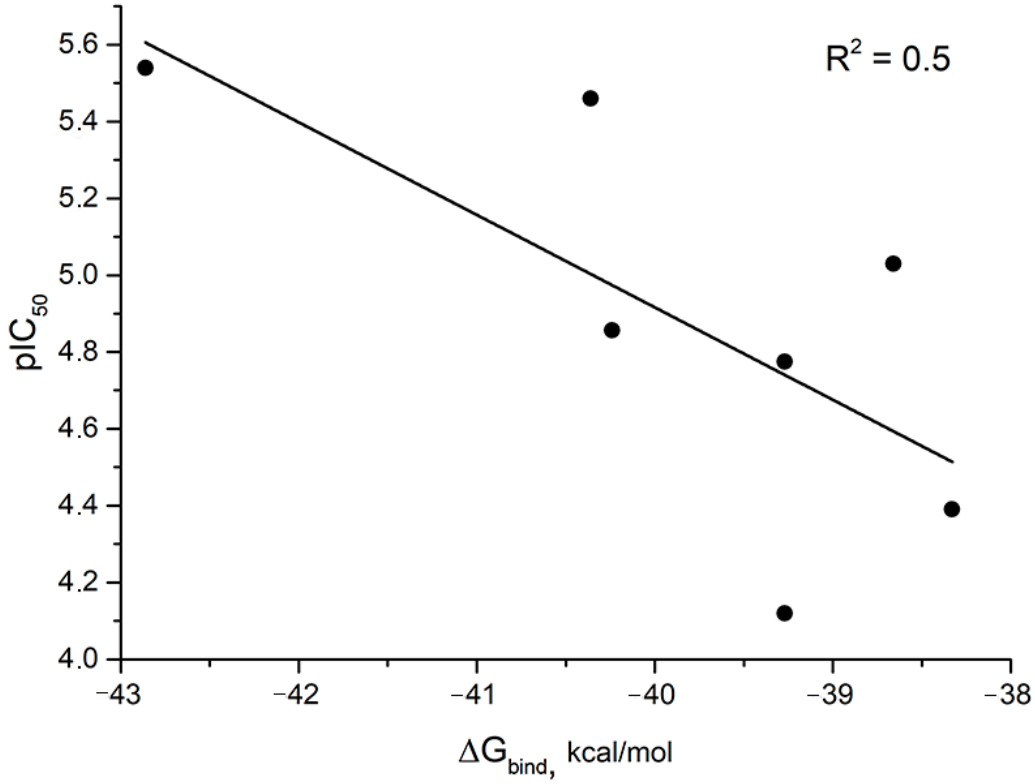

Figure 7. Correlation diagram for compounds **1**, **2**, **4**, **5R**, **5S**, **7R**, **7S**, **10R**, **10S**, **12R**, and **12S**. Gibbs binding energy is averaged for R and S isomers.

Compounds **5**R, **5S** and **7R**, and **7S** have the lowest pIC_{50} values and lowest ΔG_{bind} values for S-isomers. The R-isomers of compounds **5** and **7** have ΔG_{bind} values comparable to those of compounds **1** and **2** (Table S2).

To estimate the stability of the ligand–protein complex and the effect of ligand **2** on the side chains of amino acid residues surrounding the ligand at the binding site, molecular dynamics (MD) simulations were performed for the **2-p37** complex. The analysis of the trajectory of the MD simulation of the **2-p37** complex allows us to conclude that

the geometric parameters of system were already equalized after 60 ns of simulation (Figure S2). After aligning the geometric parameters, the position of the ligand changed during simulation within 1.5 Å, and protein position changed within 3 Å (Figure S2). The compound was located in the phospholipase region of p37 and did not diffuse into solvent during the entire simulation, as shown by data from interaction and contact graphs (Figure S3).

The time range from 60 to 150 ns was chosen to analyze the results of the molecular dynamics modeling, since, during the first 60 ns, the positions of the atoms of ligand and the main chain of protein were aligned relative to each other. A water bridge between the oxygen atom of compound **2** and Lys314 persisted for 94% of the analyzed time (Figure 8). The water–bridge contact between the nitrogen atom in the pyridine fragment and Lys281 lasted for 50% of the time analyzed. The interaction of π-cation with Lys28 was observed for 36% of the simulation time.

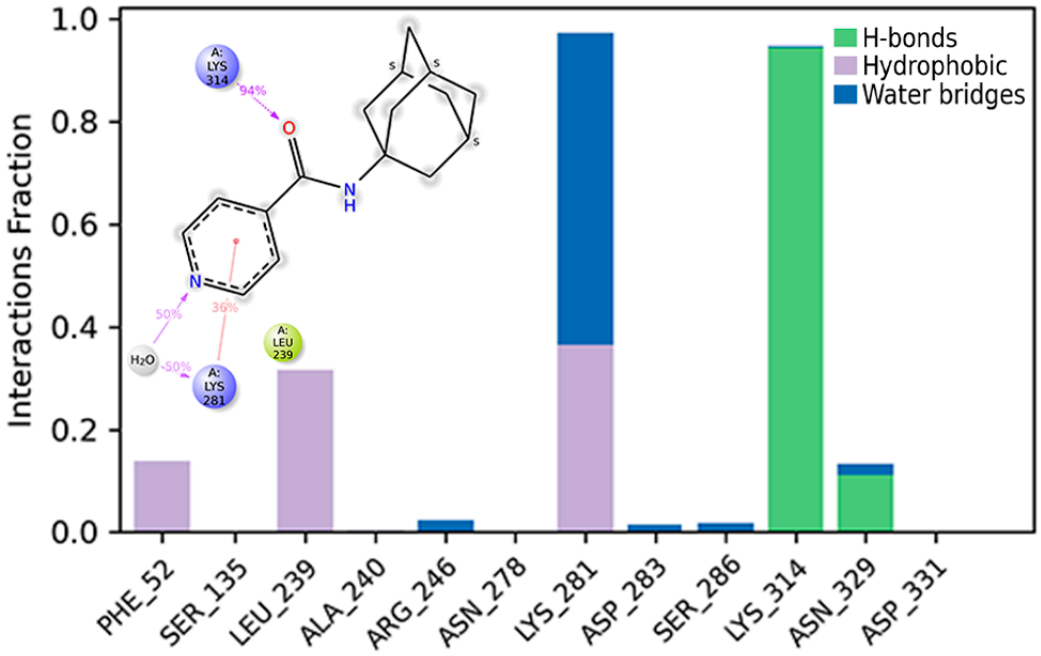

Figure 8. Histogram of the interaction of ligand atoms with the residues' binding site. The *Y*-axis represents the fraction of the simulation time (1.0 corresponds to 100%) during which the intermolecular interaction was recorded.

Thus, a combined analysis of the results of molecular modeling and biological testing allows us to conclude that the antiviral activity of compounds containing an adamantane fragment may be associated with an effect on the phospholipase activity of the viral protein p37.

4. Conclusions

Thus, in the present work, the derivatives based on 1-aminoadamantane and rimantadine were synthesized. For two heterocyclic derivatives **5** and **7**, a single-crystal X-ray diffraction study confirmed the structure, showing that the corresponding molecules in the crystalline state exist as E-isomers relative to the N1=C13 bond in the imine fragment. All synthesized agents were investigated as inhibitors of orthopoxviruses. It was shown that compounds **2**, **4** and **12** exhibited the highest activity, and the highest selectivity index, which is responsible for the efficiency and safety of a drug, was observed for the isonicotinic acid amide based on 1-aminoadamantane. The pharmacophoric analysis of the synthesized agents showed that compounds **1**, **2,** and **12,** which exhibit activity against VACV, have a

pharmacophoric profile similar to tecovirimat and therefore can be considered inhibitors of the phospholipase activity of the membrane protein p37. To evaluate the stability of the ligand–protein complex and the influence of the ligand on the side chains of the amino acid residues located at the binding site of the p37 protein, molecular dynamics simulations were carried out for the complex of agent **2** and the p37 protein. It was predicted that compound **2** is located in the region of the phospholipase domain of p37 and does not diffuse in the solvent during the entire simulation time, which allows us to conclude that the antiviral activity of compounds containing an adamantane fragment may be associated with an effect on the phospholipase activity of the viral protein p37.

Supplementary Materials: The following supporting information can be downloaded at: https://www.mdpi.com/article/10.3390/chemistry7020034/s1, File S1: the geometric parameters of the p37 protein; Table S1: Crystal data, data collection, and refinement parameters for compounds **5** and **7**; Figure S1: View of the asymmetric unit of compounds **5** and **7** with atom-numbering scheme; Table S2: Results of molecular docking, Gibbs binding energy evaluation, and comparison of the pharmacophore profiles of the molecules with the pharmacophore profile of tecovirimat; Figure S2: RMSD plot of the molecular dynamic simulation of the **2-p37** complex; Figure S3: Registration of intermolecular contacts between the atoms of ligand **2** and the amino acids of the p37 protein binding site during the molecular dynamics simulation. Synthesis of compounds **1**–**16** and NMR spectra data. Half-maximal inhibitory concentration (EC_{50}) and cytotoxic concentration (CC_{50}) for **2**, **4,** and **12**.

Author Contributions: Conceptualization, O.I.Y., S.S.B. and S.G.A.; methodology, O.I.Y., S.S.B., L.N.S., E.M.K. and V.I.P.; software, I.A.M., S.S.B. and E.M.K.; formal analysis, N.I.B., I.A.M., O.A.S. and L.N.S.; investigation, E.A.A., O.A.S., N.I.B. and E.A.D.; resources, S.G.A. and L.N.S.; data curation, S.G.A.; writing—original draft preparation, I.A.M., S.S.B., O.I.Y. and E.A.A.; writing—review and editing, O.I.Y., S.S.B. and A.Y.F.; visualization, I.A.M., E.M.K. and S.S.B.; supervision, N.F.S. and V.I.P. All authors have read and agreed to the published version of the manuscript.

Funding: Virological studies with vaccinia virus were carried out with financial support from the State assignment of the State Research Centre of Virology and Biotechnology VECTOR. This work was partially supported by the Ministry of Science and Higher Education of the Russian Federation within the governmental order for SRF SKIF Boreskov Institute of Catalysis (project FWUR-2024-0040) and within the governmental order for N.N. Vorozhtsov Novosibirsk Institute of Organic Chemistry SB RAS (project FWUE-2025-0006). The molecular dynamic study was performed under the government contract (no. 123011300044-5) of the Ministry of Science and Higher Education of the Russian Federation.

Data Availability Statement: Data are contained within the article.

Acknowledgments: The authors are grateful to the theoretical group “Quanta and Dynamics”: https://monrel.ru/about_en/ accessed on 12 December 2024.

Conflicts of Interest: The authors declare no conflicts of interest.

References

1. Boehm, E.; Summermatter, K.; Kaiser, L. Orthopox Viruses: Is the Threat Growing? *Clin. Microbiol. Infect.* **2024**, *30*, 883–887. [CrossRef]
2. Adetifa, I.; Muyembe, J.-J.; Bausch, D.G.; Heymann, D.L. Mpox Neglect and the Smallpox Niche: A Problem for Africa, a Problem for the World. *Lancet* **2023**, *401*, 1822–1824. [CrossRef]
3. Velásquez, J.S.; Herrera-Echeverría, F.B.; Porres-Paredes, H.S.; Rodríguez-Cerdeira, C. Understanding the Epidemiology of Monkeypox Virus to Prevent Future Outbreaks. *Microorganisms* **2024**, *12*, 2576. [CrossRef]
4. De Pascali, A.M.; Brandolini, M.; Peli, L.; Sambri, V.; Cricca, M.; Scagliarini, A. Zoonotic Orthopoxviruses after Smallpox Eradication: A Shift from Crisis Response to a One Health Approach. *IJID One Health* **2024**, *2*, 100018. [CrossRef]
5. Protopapas, K.; Dimopoulou, D.; Kalesis, N.; Akinosoglou, K.; Moschopoulos, C.D. Mpox and Lessons Learned in the Light of the Recent Outbreak: A Narrative Review. *Viruses* **2024**, *16*, 1620. [CrossRef] [PubMed]

6. Kumar, S.; Guruparan, D.; Karuppanan, K.; Kumar, K.J.S. Comprehensive Insights into Monkeypox (Mpox): Recent Advances in Epidemiology, Diagnostic Approaches and Therapeutic Strategies. *Pathogens* **2024**, *14*, 1. [CrossRef] [PubMed]
7. Schneider, C.P.; McDonald, M.D. "The King of Terrors" Revisited: The Smallpox Vaccination Campaign and Its Lessons for Future Biopreparedness. *J. Law Med. Ethics* **2003**, *31*, 580–589. [CrossRef]
8. Wang, J.; Shahed-AI-Mahmud, M.; Chen, A.; Li, K.; Tan, H.; Joyce, R. An Overview of Antivirals against Monkeypox Virus and Other Orthopoxviruses. *J. Med. Chem.* **2023**, *66*, 4468–4490. [CrossRef]
9. FDA News Release. FDA Approves the First Drug with an Indication for Treatment of Smallpox. Available online: https://www.fda.gov/news-events/press-announcements/fda-approves-first-drug-indication-treatment-smallpox (accessed on 24 December 2024).
10. Chen, Y.; Amantana, A.; Tyavanagimatt, S.R.; Zima, D.; Yan, X.S.; Kasi, G.; Weeks, M.; Stone, M.A.; Weimers, W.C.; Samuel, P.; et al. Comparison of the Safety and Pharmacokinetics of ST-246® after IV Infusion or Oral Administration in Mice, Rabbits and Monkeys. *PLoS ONE* **2011**, *6*, e23237. [CrossRef]
11. Mazurkov, O.Y.; Kabanov, A.S.; Shishkina, L.N.; Sergeev, A.A.; Skarnovich, M.O.; Bormotov, N.I.; Skarnovich, M.A.; Ovchinnikova, A.S.; Titova, K.A.; Galahova, D.O.; et al. New Effective Chemically Synthesized Anti-Smallpox Compound NIOCH-14. *J. Gen. Virol.* **2016**, *97*, 1229–1239. [CrossRef]
12. Hoy, S.M. Tecovirimat: First Global Approval. *Drugs* **2018**, *78*, 1377–1382. [CrossRef] [PubMed]
13. Chimerix Receives, U.S. Food and Drug Administration Approval for TEMBEXA® (Brincidofovir) for the Treatment of Smallpox. Available online: https://Ir.Chimerix.Com/News-Releases/News-Release-Details/Chimerix-Receives-Us-Food-and-Drug-Administration-Approval (accessed on 24 December 2024).
14. World Health Organization. Scientific Review of Variola Virus Research, 1999–2010. 2010. Available online: https://iris.who.int/bitstream/handle/10665/70508/WHO_HSE_GAR_BDP_2010.3_eng.pdf?sequence=1 (accessed on 24 December 2024).
15. Prichard, M.; Kern, E. Orthopoxvirus Targets for the Development of Antiviral Therapies. *Curr. Drug Target-Infect. Disord.* **2005**, *5*, 17–28. [CrossRef]
16. Parker, S.; Chen, N.G.; Foster, S.; Hartzler, H.; Hembrador, E.; Hruby, D.; Jordan, R.; Lanier, R.; Painter, G.; Painter, W.; et al. Evaluation of Disease and Viral Biomarkers as Triggers for Therapeutic Intervention in Respiratory Mousepox—An Animal Model of Smallpox. *Antiviral Res.* **2012**, *94*, 44–53. [CrossRef]
17. Ragshaniya, A.; Kumar, V.; Tittal, R.K.; Lal, K. Nascent Pharmacological Advancement in Adamantane Derivatives. *Arch. Pharm.* **2024**, *357*, 2300595. [CrossRef] [PubMed]
18. Stockdale, T.P.; Williams, C.M. Pharmaceuticals That Contain Polycyclic Hydrocarbon Scaffolds. *Chem. Soc. Rev.* **2015**, *44*, 7737–7763. [CrossRef]
19. Singh, Y.P.; Kumar, H. Recent Advances in Medicinal Chemistry of Memantine Against Alzheimer's Disease. *Chem. Biol. Drug Des.* **2024**, *104*, e14638. [CrossRef] [PubMed]
20. Jalily, P.H.; Duncan, M.C.; Fedida, D.; Wang, J.; Tietjen, I. Put a Cork in It: Plugging the M2 Viral Ion Channel to Sink Influenza. *Antiviral Res.* **2020**, *178*, 104780. [CrossRef]
21. Kuznetsov, N.Y.; Tikhov, R.M.; Godovikov, I.A.; Medvedev, M.G.; Lyssenko, K.A.; Burtseva, E.I.; Kirillova, E.S.; Bubnov, Y.N. Stereoselective Synthesis of Novel Adamantane Derivatives with High Potency against Rimantadine-Resistant Influenza A Virus Strains. *Org. Biomol. Chem.* **2017**, *15*, 3152–3157. [CrossRef]
22. Kumar, G.; Sakharam, K.A. Tackling Influenza A Virus by M2 Ion Channel Blockers: Latest Progress and Limitations. *Eur. J. Med. Chem.* **2024**, *267*, 116172. [CrossRef]
23. Lim, S.; Guo, Z.; Liu, P.; Mckay, L.G.A.; Storm, N.; Qu, M.D.; Finberg, R.W.; Somasundaran, M.; Wang, J.P. Anti-SARS-CoV-2 Activity of Adamantanes In Vitro and in Animal Models of Infection. *COVID* **2023**, *2*, 1551–1563. [CrossRef]
24. Brown, E.; Swinscoe, G.; Lefteri, D.A.; Singh, R.; Moran, A.; Thompson, R.F.; Maskell, D.; Beaumont, H.; Bentham, M.J.; Donald, C.; et al. Inhibitors of the Small Membrane (M) Protein Viroporin Prevent Zika Virus Infection. *eLife* **2024**, *13*, e68404. [CrossRef] [PubMed]
25. Kreutzberger, A.; Schröders, H.-H. Die Aliphatische Säureamidgruppierung Als Partialstruktur in Virustatika 3. Mitt. Antivirale Wirkstoffe. *Arch. Pharm.* **1974**, *307*, 766–774. [CrossRef] [PubMed]
26. Suslov, E.V.; Mozhaytsev, E.S.; Korchagina, D.V.; Bormotov, N.I.; Yarovaya, O.I.; Volcho, K.P.; Serova, O.A.; Agafonov, A.P.; Maksyutov, R.A.; Shishkina, L.N.; et al. New Chemical Agents Based on Adamantane-Monoterpene Conjugates against Orthopoxvirus Infections. *RSC Med. Chem.* **2020**, *11*, 1185–1195. [CrossRef]
27. Shiryaev, V.A.; Skomorohov, M.Y.; Leonova, M.V.; Bormotov, N.I.; Serova, O.A.; Shishkina, L.N.; Agafonov, A.P.; Maksyutov, R.A.; Klimochkin, Y.N. Adamantane Derivatives as Potential Inhibitors of P37 Major Envelope Protein and Poxvirus Reproduction. Design, Synthesis and Antiviral Activity. *Eur. J. Med. Chem.* **2021**, *221*, 113485. [CrossRef] [PubMed]
28. Mozhaitsev, E.S.; Suslov, E.V.; Rastrepaeva, D.A.; Yarovaya, O.I.; Borisevich, S.S.; Khamitov, E.M.; Kolybalov, D.S.; Arkhipov, S.G.; Bormotov, N.I.; Shishkina, L.N.; et al. Structure-Based Design, Synthesis, and Biological Evaluation of the Cage–Amide Derived Orthopox Virus Replication Inhibitors. *Viruses* **2022**, *15*, 29. [CrossRef]

29. Sokolova, A.S.; Kovaleva, K.S.; Kuranov, S.O.; Bormotov, N.I.; Borisevich, S.S.; Zhukovets, A.A.; Yarovaya, O.I.; Serova, O.A.; Nawrozkij, M.B.; Vernigora, A.A.; et al. Design, Synthesis, and Biological Evaluation of (+)-Camphor- and (−)-Fenchone-Based Derivatives as Potent Orthopoxvirus Inhibitors. *ChemMedChem* **2022**, *17*, e202100771. [CrossRef]
30. Chen, Y.; Honeychurch, K.M.; Yang, G.; Byrd, C.M.; Harver, C.; Hruby, D.E.; Jordan, R. Vaccinia Virus P37 Interacts with Host Proteins Associated with LE-Derived Transport Vesicle Biogenesis. *Virol. J.* **2009**, *6*, 44. [CrossRef]
31. Sen Gupta, P.S.; Panda, S.K.; Nayak, A.K.; Rana, M.K. Identification and Investigation of a Cryptic Binding Pocket of the P37 Envelope Protein of Monkeypox Virus by Molecular Dynamics Simulations. *J. Phys. Chem. Lett.* **2023**, *14*, 3230–3235. [CrossRef]
32. Duraffour, S.; Lorenzo, M.M.; Zöller, G.; Topalis, D.; Grosenbach, D.; Hruby, D.E.; Andrei, G.; Blasco, R.; Meyer, H.; Snoeck, R. ST-246 Is a Key Antiviral to Inhibit the Viral F13L Phospholipase, One of the Essential Proteins for Orthopoxvirus Wrapping. *J. Antimicrob. Chemother.* **2015**, *70*, 1367–1380. [CrossRef]
33. Jordan, R.; Leeds, J.M.; Tyavanagimatt, S.; Hruby, D.E. Development of ST-246® for Treatment of Poxvirus Infections. *Viruses* **2010**, *2*, 2409–2435. [CrossRef]
34. Akishina, E.A.; Dikusar, E.A.; Kurman, P.V.; Potkin, V.I. Synthesis of Novel Rimantadine and Adamantane-1-Carboxylic Acid Derivatives with 1,2-Azole Fragments. *Proc. Natl. Acad. Sci. Belarus Chem. Ser.* **2023**, *59*, 211–224. [CrossRef]
35. Selivanov, B.A.; Tikhonov, A.; Belanov, E.F.; Bormotov, N.I.; Kabanov, A.S.; Mazurkov, O.Y.; Serova, O.A.; Shishkina, L.N.; Agafonov, A.P.; Sergeev, A.N. Synthesis and Antiviral Activity of 1-Aryl-3-{3,5-Dioxo-4-Azatetracyclo[5.3.2.02,6.08,10]-Dodec-11-En-4-Yl}ureas. *Khimiko-Farmatsevticheskii Zhurnal* **2017**, *51*, 13–17. [CrossRef]
36. Lu, C.; Wu, C.; Ghoreishi, D.; Chen, W.; Wang, L.; Damm, W.; Ross, G.A.; Dahlgren, M.K.; Russell, E.; Von Bargen, C.D.; et al. OPLS4: Improving Force Field Accuracy on Challenging Regimes of Chemical Space. *J. Chem. Theory Comput.* **2021**, *17*, 4291–4300. [CrossRef] [PubMed]
37. Johnston, R.C.; Yao, K.; Kaplan, Z.; Chelliah, M.; Leswing, K.; Seekins, S.; Watts, S.; Calkins, D.; Chief Elk, J.; Jerome, S.V.; et al. Epik: P K a and Protonation State Prediction through Machine Learning. *J. Chem. Theory Comput.* **2023**, *19*, 2380–2388. [CrossRef]
38. Mirdita, M.; Schütze, K.; Moriwaki, Y.; Heo, L.; Ovchinnikov, S.; Steinegger, M. ColabFold: Making Protein Folding Accessible to All. *Nat. Methods* **2022**, *19*, 679–682. [CrossRef]
39. Rothkirch, A.; Gatta, G.D.; Meyer, M.; Merkel, S.; Merlini, M.; Liermann, H.-P. Single-Crystal Diffraction at the Extreme Conditions Beamline P02.2: Procedure for Collecting and Analyzing High-Pressure Single-Crystal Data. *J. Synchrotron Radiat.* **2013**, *20*, 711–720. [CrossRef]
40. CrysAlisPro 171.43.143a, Rigaku Oxford Diffraction, 2023. Available online: https://www.rigaku.com/products/crystallography/crysalis (accessed on 9 December 2024).
41. Sheldrick, G.M. SHELXT–Integrated Space-Group and Crystal-Structure Determination. *Acta Crystallogr. Sect. A Found. Adv.* **2015**, *71*, 3–8. [CrossRef]
42. Sheldrick, G.M. Crystal Structure Refinement with SHELXL. *Acta Crystallogr. Sect. C Struct. Chem.* **2015**, *71*, 3–8. [CrossRef]
43. Dolomanov, O.V.; Bourhis, L.J.; Gildea, R.J.; Howard, J.A.K.; Puschmann, H. OLEX2: A Complete Structure Solution, Refinement and Analysis Program. *J. Appl. Crystallogr.* **2009**, *42*, 339–341. [CrossRef]
44. Spek, A.L. Structure Validation in Chemical Crystallography. *Acta Crystallogr. Sect. D Biol. Crystallogr.* **2009**, *65*, 148–155. [CrossRef]
45. Macrae, C.F.; Sovago, I.; Cottrell, S.J.; Galek, P.T.A.; McCabe, P.; Pidcock, E.; Platings, M.; Shields, G.P.; Stevens, J.S.; Towler, M.; et al. Mercury 4.0: From Visualization to Analysis, Design and Prediction. *J. Appl. Crystallogr.* **2020**, *53*, 226–235. [CrossRef] [PubMed]
46. Fridman, A.L.; Sivkova, M.P.; Zalesov, V.S.; Dolbilkin, K.V.; Moiseev, I.K.; Doroshenko, R.I.; Manzhelevskaya, É.V. Synthesis and Biological Activity of Adamantane Derivatives. *Pharm. Chem. J.* **1979**, *13*, 1241–1246. [CrossRef]
47. Okawara, T.; Islam, R.; Hossain, M.I.; Okamoto, Y.; Nagamatsu, T.; Anraku, K. ChemInform Abstract: Facile Synthesis of 2-Phenylquinoline-4-carboxamide Derivatives with Variant Structural Features. *ChemInform* **2014**, *45*, 32. [CrossRef]
48. Borisevich, S.S.; Gorokhov, Y.V.; Arkhipov, S.G. Binding Site of Tecovirimat, Inhibitor of the P37 Membrane Protein of Orthopox Viruses. *J. Struct. Chem.* **2024**, *65*, 776–785. [CrossRef]

Disclaimer/Publisher's Note: The statements, opinions and data contained in all publications are solely those of the individual author(s) and contributor(s) and not of MDPI and/or the editor(s). MDPI and/or the editor(s) disclaim responsibility for any injury to people or property resulting from any ideas, methods, instructions or products referred to in the content.